Room temperature huge magnetocaloric properties in low hysteresis ordered Cu-doped Ni-Mn-In-Co alloys

Paulo La Roca, Javier López-García, Vicente Sánchez-Alarcos, Vicente Recarte, José Alberto Rodríguez-Velamazán, José Ignacio Pérez-Landazábal

PII: S0925-8388(22)02534-8

DOI: https://doi.org/10.1016/j.jallcom.2022.166143

Reference: JALCOM166143

To appear in: *Journal of Alloys and Compounds*

Received date: 29 April 2022
Revised date: 7 June 2022
Accepted date: 30 June 2022

Please cite this article as: Paulo La Roca, Javier López-García, Vicente Sánchez-Alarcos, Vicente Recarte, José Alberto Rodríguez-Velamazán and José Ignacio Pérez-Landazábal, Room temperature huge magnetocaloric properties in low hysteresis ordered Cu-doped Ni-Mn-In-Co alloys, *Journal of Alloys and Compounds,* (2022) doi:https://doi.org/10.1016/j.jallcom.2022.166143

Room temperature huge magnetocaloric properties in low hysteresis ordered Cu-doped Ni-Mn-In-Co alloys.

Paulo La Roca *[a,b,c] , Javier López-García [a,d] , Vicente Sánchez-Alarcos [a,c] , Vicente Recarte [a,c] , José Alberto Rodríguez-Velamazán[e], José Ignacio Pérez-Landazábal [a,c]

[a] Institute for Advanced Materials and Mathematics (INAMAT^2), Universidad Pública de Navarra, Campus de Arrosadia, Pamplona 31006, Spain
[b] Centro Atómico Bariloche (CNEA), CONICET, Bariloche 8400, Argentina
[c] Science Department, Universidad Pública de Navarra, Campus de Arrosadia, Pamplona 31006, Spain
[d] Department of Physics, Faculty of Science, University of Oviedo, Oviedo 33007, Spain
[e] Institut Laue Langevin, 71, Avenue des Martyrs, 38042 Grenoble Cedex, France

Keywords: Martensitic transformation, Order-disorder phenomena, Heusler Alloys, Shape Memory Alloys, Magnetocaloric effect.

Abstract: The reduction of the thermal hysteresis in first order magnetostructural transition is a determining factor to decrease energy losses and to improve the efficiency of magnetocaloric cooling based systems. In this work, a Cu doped NiMnInCo metamagnetic shape memory alloy (MMSMA) exhibiting a narrow thermal hysteresis (around 5 K) at room temperature has been designed. In this alloy, the induced $L2_1$ ordering process affects the phase stability in an unusual way compared to that observed in NiMnInCo and other NiMn based alloys. This ordering produces an increase in the Curie temperature of the austenite but hardly affects the martensitic transformation temperatures. As a consequence, the ordering increases the magnetization of the austenite without changing the transformation temperatures, doubles the sensitivity of the transformation to magnetic fields (the Claussius-Clapeyron slope goes from 2.1 to 3.9 K/T), improves the magnetocaloric effect, the reversibility and finally, enhances the refrigeration capacity. In addition, the magnetic hysteresis losses are among the lowest reported in the literature and the effective

cooling capacity coefficient RC_{eff} reaches 86 J/Kg for 2T (15% higher than those found in Ni-Mn based alloys) and 314 J/Kg for 6T fields. Therefore, the ordered alloy possesses an excellent combination of low thermal hysteresis and high RC_{eff}, not achieved previously in metamagnetic shape memory alloys near room temperature.

1. Introduction

Refrigeration plays an increasingly vital role in many domains of our daily lives such as, food preservation and production, air-conditioning, medicine, and more. Today, about 15%-30% of the world's electricity consumption is used in refrigeration and air-conditioning systems [1]. The current technology based on vapour-compression uses volatile substances that strongly damage the ozone layer and is reaching its technical limits of efficiency to achieve additional improvements [2]. For this reason, conventional vapour-compression cooling systems must be replaced in the next years. To solve this problem, near-room-temperature cooling with heat pumping based on solid caloric materials holds great promise as a game changer [3]. In this way, magnetocaloric (MC) materials focused the greatest interest of the scientific community in order to develop affordable and low cost magnetocaloric materials that exhibit strong caloric effect and do not contain expensive, toxic or rare-earth elements [4-7]. In MC materials an adiabatic temperature change ΔT_{ad} can be induced as a result of magnetothermal interplay between the magnetic moments and the atomic lattice vibrations (phonons). Interesting and promising magnetocaloric materials are Shape memory alloys (SMA) [8]. SMAs are characterized by their ability to undergo large controlled and reversible strains under temperature variations, mechanical load or magnetic fields application. These phenomena are linked to the martensitic transformation (MT), a diffusionless first-order solid-to-solid phase transformation characterized by a coordinated movement of atoms. If the magnetic properties of both phases were sufficiently different, a magnetostructural MT can be induced by external magnetic fields. This is

the case of Heusler MMSMA Ni-Mn-X (X = In, Sn, Sb) where on cooling the MT occurs between a ferromagnetic austenite and a near paramagnetic martensite [6]. In particular, the MSMA (Ni-Mn-In-Co and others) combine a number of advantages: 1) high adiabatic temperature change in low field, 2) easy fabrication, 3) good oxidation resistance, 4) better mechanical properties than intermetallic materials, 5) do not contain rare-earth, precious, toxic or expensive elements. However, there are challenges to solve: 1) reduction of the thermal and magnetic hysteresis of the MT that produces energy losses, 2) achievement of reversible transformations with the highest MCE possible.

The reduction of thermal hysteresis is a determining factor to decrease energy losses and to improve the transformation reversibility [9, 10]. Recently, the effects of the thermal hysteresis on the efficiency of first-order caloric materials were analyzed by T. Hess et al. [11] and demonstrate that the thermal hysteresis needs to be further reduced to compete with the efficiency of gas compressor-based systems.

In this way, works reported by Zhao et al [12,13] show an interesting reduction of thermal hysteresis effect related to a partial substitution of Cu in NiMnGa alloys. Later, works reported by Zuo et al [14-16] show an interesting strategy to optimize magnetism and hysteresis with a partial substitution of Cu in NiMnInCo alloys. Particularly, for $Ni_{45}Co_5Mn_{36}In_{14-x}Cu_x$ (x = 0–1.5) the presence of Cu can enhance the geometrical compatibility between austenite and martensite, bringing about a remarkable reduction of thermal hysteresis [15]. Likewise, the $Ni_{45}Co_5Mn_{36}In_{13.3}Cu_{0.7}$ alloy has been shown to exhibit an excellent reversible magnetocaloric effect, with refrigeration capacity values among the highest ones reported in Ni-Mn-based alloys. In the present work, a NiMnInCoCu alloy transforming near room temperature has been designed using a content of Cu larger than that reported in the literature. The influence of the atomic ordering has been analyzed and correlated to the magnetocaloric characteristics of the alloy.

2. Experimental method

A Cu doped $Ni_{44.5}Mn_{35.5}In_{13.5}Co_4Cu_{2.5}$ alloy has been elaborated by arc-melting from pure elements. The elaborated polycrystalline ingot was homogenized during 48 hrs. at 1173 K and then quenched into iced water to retain a high degree of long-range atomic disorder. The Mn, Ni and In contents were selected to obtain an electron concentration close to 7.93 where the MT occurs near room temperature [17]. On the other side, a higher content of Cu with respect to previously reported alloys [14,15] and a smaller Co concentration was used as a strategy to obtain low thermal hysteresis [18]. Chemical composition was checked by electron dispersive spectroscopy (EDS) using a Zeiss EVO 15 VP Scanning Electron Microscope.

The MT was characterized by differential scanning calorimetry (Q-1000 DSC, TA Instruments), on heating-cooling cycles performed at 10 K/min [19].

Temperature dependence of magnetization measurements at 2 K/min under different applied fields and field dependence of the magnetization measurements at different constant temperatures were performed by SQUID magnetometry (QD MPMS XL-7).

Neutron scattering experiments were carried out at Institut Laue-Langevin, in Grenoble, France. The structural features were analyzed by powder neutron diffraction, using data collected in D1B (λ = 1.28 Å). Diffraction data were analyzed using Fullprof Suite [20]. In situ temperature-dependent measurements of a NiMnInCoCu powder alloy were carried out on heating from 250K up to 673K and on subsequent cooling down to 260K, at a rate of 1K/m, covering the structural changes in austenite and martensite phases. The powder samples were prepared by manually milling (agate mortar) selecting sieved particles bellow 400 µm. Then, the powders were annealed at 410 K during 10 min to eliminate the possible presence of mechanically stabilized martensite during grinding [21]. The total disappearance of this type of martensite was verified by DSC and confirmed by neutron diffraction results.

3. Results and discussion

3.1 Phase stability

Several consecutive heating/cooling thermal cycles have been performed on the as-quenched sample (AQ) to determine the effect of the ordering process on the transformation temperatures and on the entropy change. The cycles have been carried out "*In situ*" in the DSC from a temperature below the MT to a temperature T_{aging} above MT, higher and higher in each new cycle. The sequence is performed in such a way that each cycle can be considered as a new aging treatment (at T_{aging}). Figure 1.a shows the DSC corresponding to the thermal excursions as well as the respective qualitative evolution of the Curie and MT temperatures with T_{aging}. The comparison with the NiMnInCo behavior is also included as an inset [22]. The variation of the martensitic start temperature (ΔT_m,) and the variation of the Curie temperature (ΔT_C) are shown in Figure 1.b where black data correspond to a NiMnInCo alloy and red data to the NiMnInCoCu alloy. The Curie temperature increases on heating between 500 K and 650 K pointing to an increase of the atomic order (confirmed in ternary NiMnIn and quaternary NiMnInCo alloys [22,23], but the MT temperature remains almost constant. This is unexpected since very large shifts of the MT, up to 70 K, are observed in similar NiMnIn and NiMnInCo alloys subjected to exactly the same thermal treatments [22-25]. Previous works shows that the shift in MT are related to L21 ordering and it´s explained from the magnetic contribution to the Gibbs free energy change [22-25].

In the following, and in order to define an easily reproducible high ordered state reference, a heat treatment at 673 K (400ºC) for 15 min has been performed, for this, the ordered samples will be referred as ORD. Figure 1.b, shows the corresponding values of ΔT_c and ΔT_m that effectively coincide with the asymptotic values obtained from successive treatments described earlier.

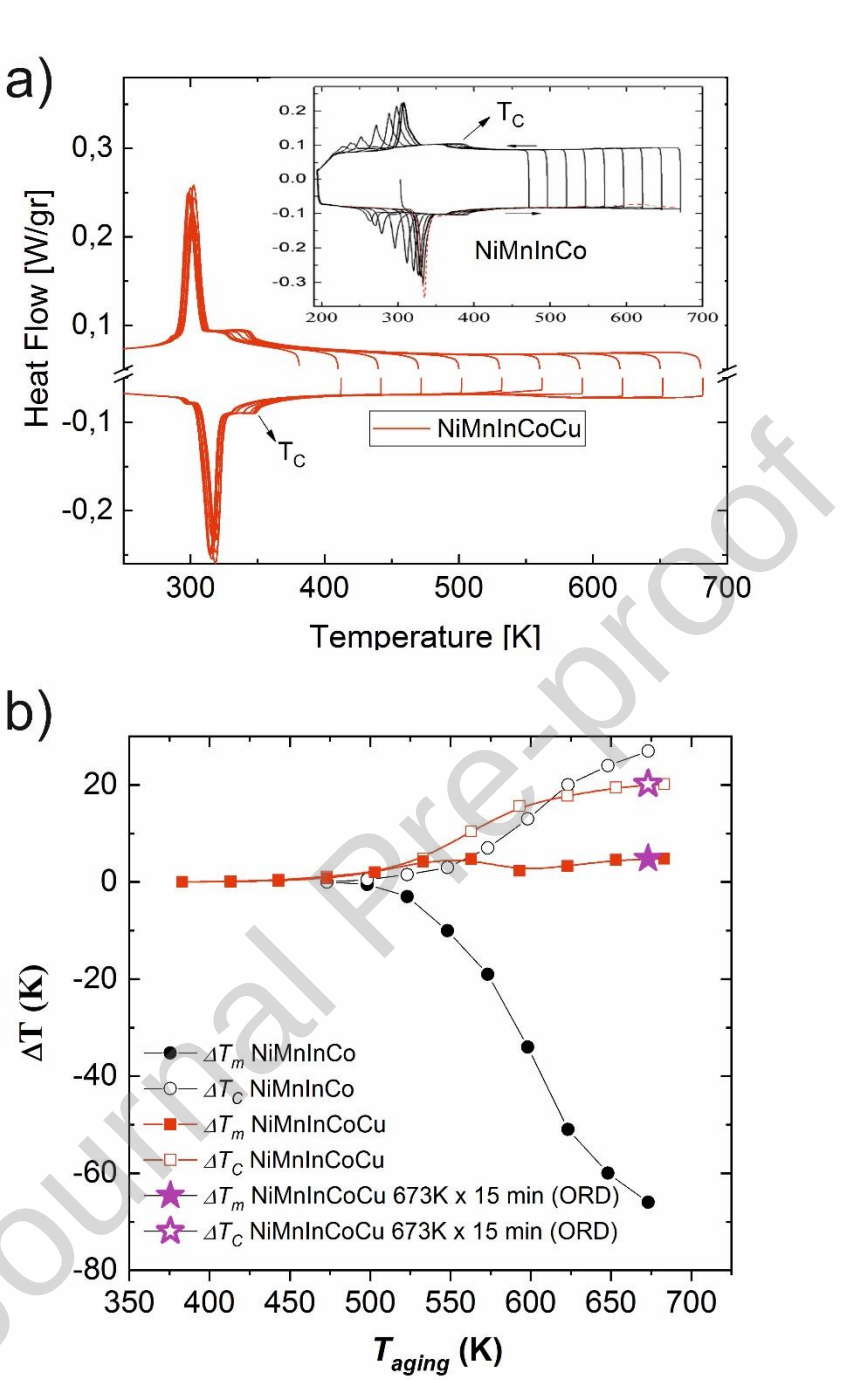

Figure 1. a) DSC measurements of consecutive heating/cooling DSC thermal cycles at different maximum temperatures for each cycle (T_{aging}), the inset corresponds to a comparison with NiMnInCo alloys [22] b) Variation of martensitic start temperature (ΔT_m,) and the variation of the Curie temperature (ΔT_C) as function of T_{aging} for NiMnInCo, NiMnInCoCu and ORD samples.

3.2 Structural parameters and ordering effects

In order to understand the unexpected phase stability behavior, in situ neutron diffraction experiments were conducted. Neutron Powder Diffraction (NPD) patterns in

$L2_1$ (Fm3m space group) austenite (400 K) for AQ and ORD samples are shown in figure 2. Simulated full ordered and full 2nd neighbors disordered patterns are also included. The texture present on the samples does not allow a reliable Rietveld refinement to evaluate site occupancies and consequently the exact order degree. However, the ratio between the intensities of the $[111]_{L21}$ and $[222]_{B2}$ reflections is texture independent (correspond to parallel planes). Therefore, all patterns were normalized to the $[222]_{B2}$ peak intensity and the $[111]_{L21}$ reflection allows to estimate the degree of $L2_1$ atomic order. Comparing the relative intensities, the ORD sample shows approximately a 60% of the maximum possible ordering according to composition (with respect to the Full order simulation) and the AQ sample represents only a 25%. As will be shown later, the martensite and austenite structures were analyzed in AQ and ORD samples. The results, corroborates the L21 ordering during thermal treatments without any changes in martensite structure as has been reported before [26]. So, ageing increases the atomic order and the Curie temperature of the austenite but leaves the transformation temperatures unchanged. As mentioned before, this is an unexpected behavior due to the magnetic contribution to Gibbs energy [21-25]. However, can be related to a simultaneously secondary effect like annihilation of quenched-in vacancies [27] or change of the average L21 order domain size as has been reported recently for NiMnInCo alloys [28].

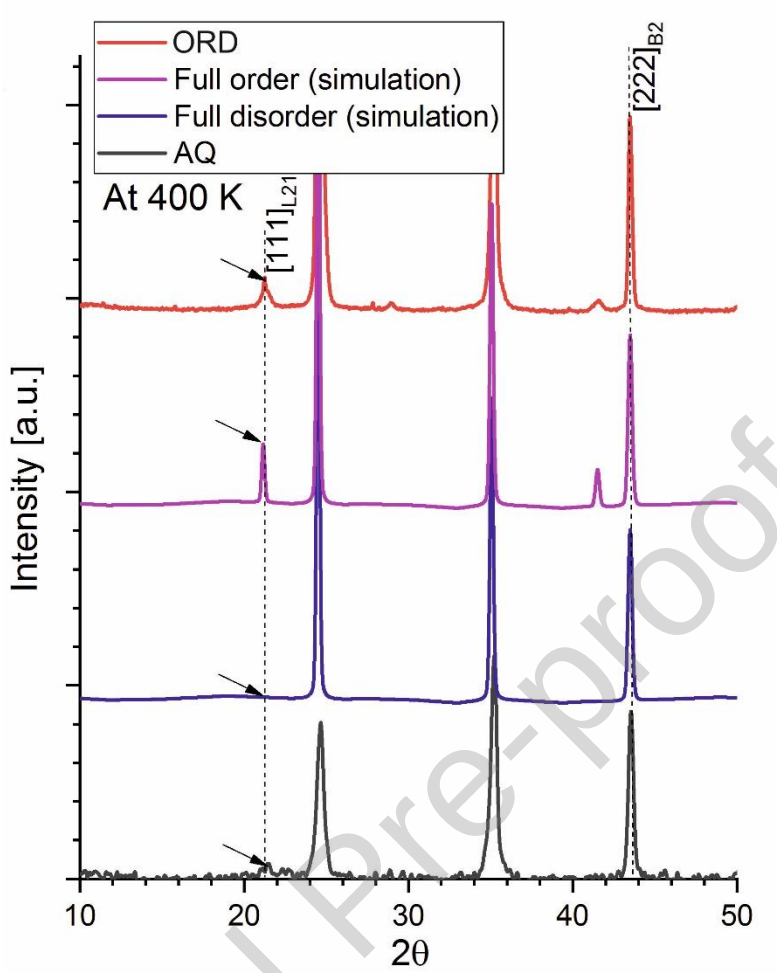

Figure 2. Neutron diffraction patterns obtained at 400 K of AQ, and ORD samples. Full order and full disorder simulation patterns were also included. The y-axes scale of each pattern were modified in order to obtain a similar high for $[222]_{B2}$ peak.

On the other side, as we described in experimental method, the structural modifications were followed by in-situ powder neutron diffraction experiments. The martensite phase corresponds to a P2/m monoclinic structure (with triple modulation, N=3) in both AQ and ORD samples. Table 1, shows the lattice parameters of the cubic austenite (a_0) and monoclinic martensite.

Table 1. Lattice parameters and error (indicated between parentheses) of both structures for samples AQ, ORD and NiMnInCo [21] obtained by neutron diffraction.

	a_0	a	b	c	β
AQ	5,98738 (52)	4.3259 (7)	5.5914 (35)	13.2395 (79)	93.5900 (163)
ORD	6.006 (1)	4.4025 (4)	5.5951 (4)	12.995809 (93)	93.5098 (52)
NiMnInCo	5.9840	4.3260	5.5620	13,174	94.0

Although Landau's phenomenological theory and experimental results show that the thermal hysteresis can disappear of under a field of 30 T [29], thermal hysteresis is one of the main drawbacks for cyclical applications of magnetocaloric materials based on first-order transformations. Crystallographic theory of martensitic transformation [30, 31] indicates that internal stresses and irreversible processes associated to martensitic transformation can be reduced by improving the geometric compatibility between the austenite and the martensitic structures, thereby reducing the thermal hysteresis. In particular, the compatibility between structures can be analyzed through the transformation stretch tensor **U** [31-35]. The determination of tensor U relies on the crystalline structures and their lattice parameters. In the present case, where a cubic (Fm3m) to monoclinic (P2/m) phase transformation occurs, there are 12 stretch tensors related by symmetry that correspond to 24 possible martensitic variants [31, 32]. All these tensors have the same eigenvalues. One of these possible tensors is:

$$U = \begin{pmatrix} \tau & \sigma & 0 \\ \sigma & \rho & 0 \\ 0 & 0 & \gamma \end{pmatrix}$$

Where:

$$\tau = \frac{\alpha^2 + \gamma^2 + 2\alpha\gamma(sin\beta - cos\beta)}{2\sqrt{\alpha^2 + \gamma^2 + 2\alpha\gamma(sin\beta)}}$$

$$\rho = \frac{\alpha^2 + \gamma^2 + 2\alpha\gamma(sin\beta + cos\beta)}{2\sqrt{\alpha^2 + \gamma^2 + 2\alpha\gamma(sin\beta)}}$$

$$\sigma = \frac{\alpha^2 - \gamma^2}{2\sqrt{\alpha^2 + \gamma^2 + 2\alpha\gamma(sin\beta)}}$$

Being

$$\delta = \frac{b}{a_0}$$

$$\gamma = \sqrt{2}\frac{c}{Na_0}$$

$$\alpha = \sqrt{2}\frac{a}{Na_0}$$

A modulation N=3 according to the martensitic structure has been used in the present case. According to the theory, improved compatibility occurs when the middle eigenvalue λ_2 of the diagonal matrix is closer to one. In fact, a strong correlation between the hysteresis width and λ_2 has been widely reported in Ni-Mn-*X*-based Heusler alloys [14, 15, 31, 35, 36]. Using the lattice parameters from Table 1, we calculate the components of the U tensor and the corresponding eigenvalues, shown in Table 2 for AQ and ORD samples. The hysteresis of the transformation (T_{hys}) measured from low field magnetization curves (see figure 3a, below) is also included in the table.

Table 2: Calculated components of the U transformation tensor and the eigenvalues compared to thermal hysteresis T_{hys} for AQ, ORD and NiMnInCo [21]

	τ	σ	ρ	γ	λ_1	λ_2	λ_3	T_{hys} [K]
AQ	0.9992481	-0.0103112	1.06389845	1.0423858	1.0424	0.9978	1.0655	5.1
ORD	0.9963629	0.00831159	1.05934224	1.0200271	1.0200	0.9953	1.0604	6.2
NiMnInCo	0.9935192	-0.0077249	1.065414793	1.0378146	1.0378	0.9927	1.0662	12.3

The middle eigenvalues (λ_2) show a congruent correlation with the thermal hysteresis; the hysteresis decreases as the λ_2 parameter approaches to 1, i.e. consistent with a better structural compatibility between martensite and austenite [6, 18, 37, 38]. It is well known that NiMnInCo alloys display differences in thermal hysteresis due to composition changes [18], but it is interesting to note that the addition of a small quantity of Cu improves the structure compatibility and decreases the thermal hysteresis (see table 2, where parameters of NiMnInCo alloys are also included) [14,

15]. In this sense, the addition of 10% of Pt to NiMnIn alloys also decreases the thermal hysteresis to 4K with λ_2=0.9982 [36], but Pt increases the alloy cost in a remarkable way.

3.3 Magnetocaloric properties

Magnetization versus temperature curves under 100 Oe and 6T applied magnetic fields are shown in figure 3a and 3b, respectively. The ordering process leads to an increase in global magnetization, coherent with the increase in the Curie temperature. The high field (6T) magnetization change (ΔM) linked to the MT is 68 and 72 emu/gr in the AQ and ORD samples, respectively.

Figure 3c shows the DSC of the AQ and ORD samples, where the transformation enthalpy (ΔH) reduces from 8.4 J/g to 5.7 J/g for ORD sample as a consequence of the ordering process. This change in enthalpy is understandable given the opposing contributions to magnetic Gibbs free energy [24, 25]. Therefore, the heat exchanged during field induced martensitic transformation should be smaller in the ordered alloy representing a drawback to improve the magnetocaloric effect. However, ordering induces the combination of a slight increase in the magnetization change and a decrease in enthalpy associated with the transformation, and consequently the order increases the Clausius-Clapeyron slope ($\partial T_M/\partial B$) that is proportional to the ratio $\Delta M/\Delta H$ [39-41]. So, the shift of the MT temperature with the applied field increases with the atomic order as shown comparatively in figures 3a and 3b.

The effect of the magnetic field on the MT was studied using M(T) curves under different magnetic fields. The peak in the derivative of the M(T) curve (see inset in figure 3d) has been used to characterize the variation of the transformation temperatures (T_{peak}) with the applied field as shown in Figure 3d The variation ($\partial T_M/\partial B$) changes from 2.1 K/T for the AQ sample to 3.9 K/T for the ordered ORD sample,

practically doubling the sensitivity of the alloy to a magnetic field. This result acquires relevance since ordering occurs without modifying the transformation temperatures, unlike what happens in other NiMnIn alloys [22-25]. Additionally, the increase of the magnetic field sensitivity ($\partial T M / \partial B$) and the low thermal hysteresis found in the ORD sample are beneficial for maximizing the fraction induced by the magnetic field and for a better reversibility, as we will discuss later [9].

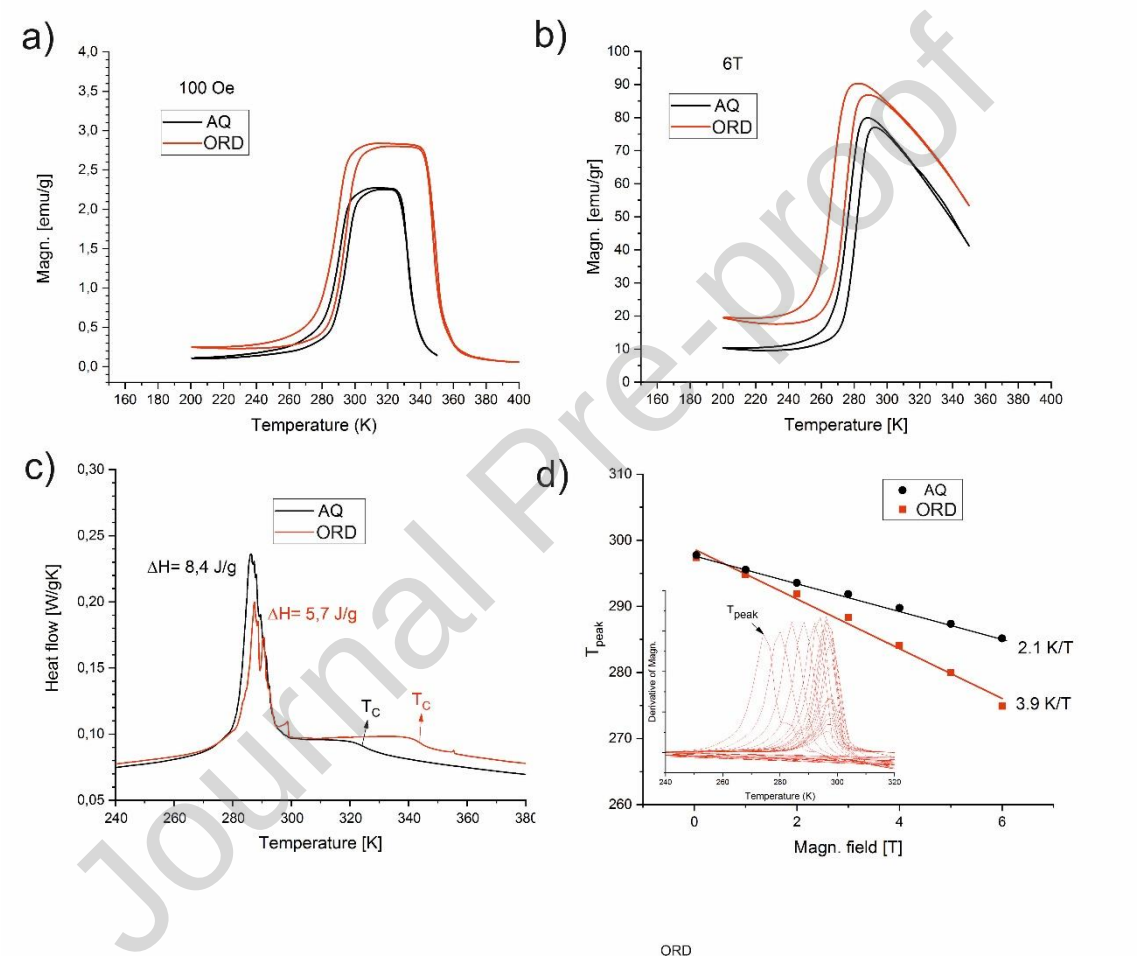

Figure 3. a) M(T) curves under 100 Oe applied field for the AQ, and ORD bulk samples b) Same at 6T c) DSC thermogram for AQ and ORD alloys during heating showing the difference on the enthalpy. d) T_{peak} vs magnetic field for AQ and ORD samples showing the Claussius-Clapeyron relationship. The inset shows the temperature dependence of the derivative M(T) at different applied fields where the maximum of the peak corresponds to a T_{peak}

In order to get deeper into the effect of atomic ordering on the magnetocaloric properties, the isothermal entropy changes, ΔS_{iso} (T) were obtained from M(T) curves measured on heating using the Maxwell´s relation:

$$\Delta S_{iso}(T) = \int_0^H \left(\frac{\partial M}{\partial T}\right)_H dH$$

Figures 4a and 4b show the isothermal entropy change as a function of temperature for applied fields between 1 and 6 T for samples AQ and ORD, respectively. Both show similar maximum ΔS_{iso} (~20 J/KgK). Therefore, although the ordered sample has a lower MT enthalpy change (figure 3c), the higher field-induced transformed fraction of the ordered alloy (higher $\partial T_M/\partial B$) compensates the martensitic transformation entropy change. Another interesting point related to a higher $\partial T_M/\partial B$ of ORD sample is that a high entropy change can be achieved over a wide temperature range of about 27 K (determined from FWHM of $\Delta S_{iso}(T)$ peak). The wide range for the magnetocaloric effect is an important parameter in case of cascade cooling and increase the refrigeration capacity as can be seen below.

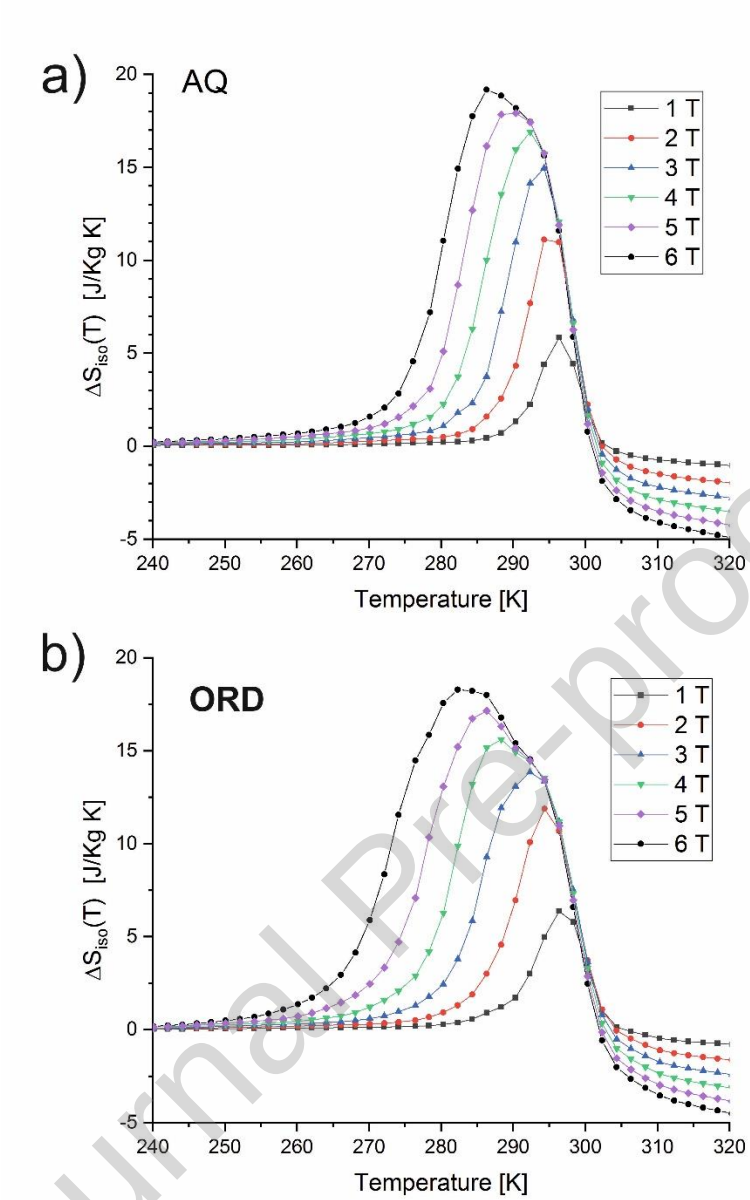

Figure 4. Isothermal entropy change $\Delta S_{iso}(T)$ as a function of temperature for different magnetic applied field between 1T and 6T a) AQ sample b) ORD sample.

The refrigeration capacity *RC*, which represents the maximum amount of thermal energy transferable between the cold (T_{cold}) and hot (T_{hot}) sources in a thermodynamic cycle [42], can be computed using:

$$RC = \int_{T_{cold}}^{T_{hot}} \Delta S_{iso}(T)\, dT$$

where the temperature integration range can be estimated from the full width at half maximum (δ_{FWHM}) of the $\Delta S_{iso}(T)$ curves (figures 4a and 4b). Figure 5a shows the RC for ORD and AQ samples for different fields. The ordered sample clearly shows a greater cooling capacity for all the applied fields, improving the magnetocaloric response from an application point of view. Particularly for 2T and 6T, the enhancement represents around 25%. Nevertheless, larger RC have been reported in the literature [15] but the low thermal hysteresis that the ordered alloy shows has an additional advantage; the hysteresis losses (HL) of the magnetic field induced cycle are smaller. HL(T) can be estimated from the area enclosed by the hysteresis loops M(H) at constant temperature and depends on the maximum applied magnetic field as shown in Figure 5b. Comparing the M(H) behavior of the ORD (red curve) with AQ (grey curve), it can be seen that the ordered alloy possess a narrower cycle that can be related with a better reversibility after removing the applied magnetic field (6T). So the HL(T) can be reduced with ordering as will be shown later on figure 5c. This point is very interesting because the AQ sample displays a lower thermal hysteresis than ORD, but this sample shows a double magnetic field sensitivity (higher $\partial T_M/\partial B$).

Figure 5c shows the temperature dependence of HL(T) for AQ and ORD samples under maximum magnetic field of 6 T. Alloys with the largest reported RC are also shown in the figure for comparison. As mentioned before, the hysteresis losses is lower in the ORD alloy than in AQ sample, and remarkably lower than all the others (even comparing the cycle obtained at 6T with bibliography data obtained at 5T) and this improvement should be attributed to a reduced thermal hysteresis and a high $\partial T_M/\partial B$ [9]. It is also important to highlight the close to room temperature working range of the present alloy.

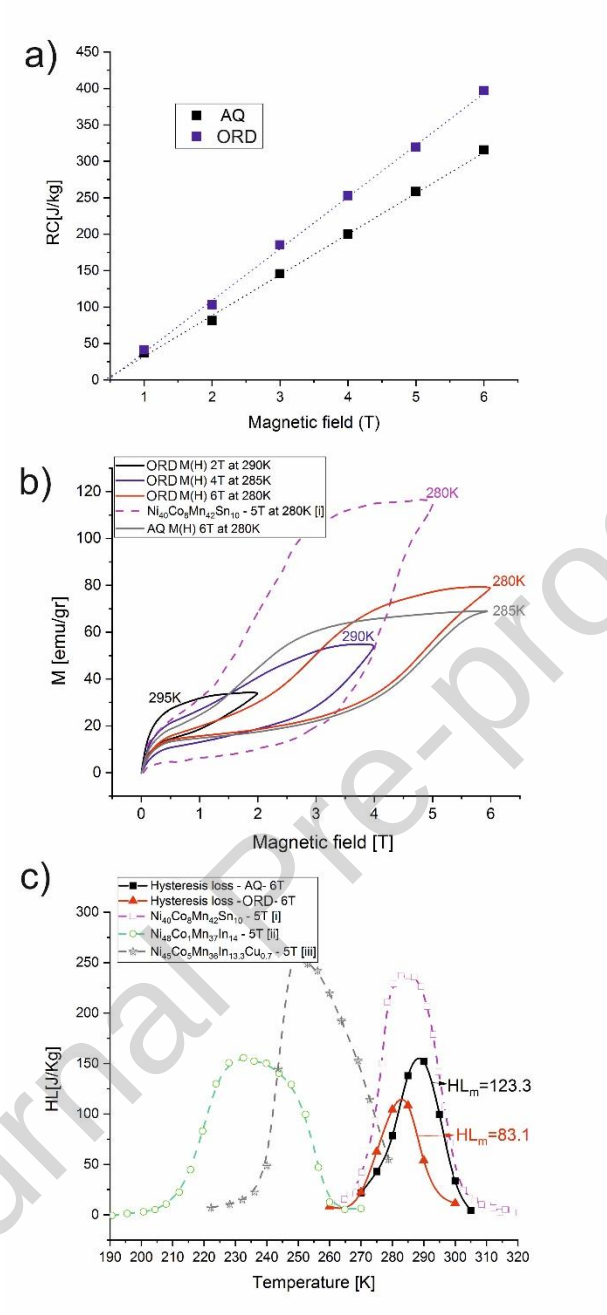

Figure 5. a) Refrigeration capacity RC as function of the magnetic field for AQ (black squares) and ORD (blue triangles) samples. b) Hysteresis loops M(H) at different maximum applied magnetic field, each temperature correspond to maximum HL c) Hysteresis Loss of AQ (black) and ORD (red) samples measured at 6 T compared with data obtained from references: i [43], ii [44], iii [15] at 5T.

The effective refrigeration capacity defined as $RC_{eff} = RC - HL_m$ where HL_m is the average hysteresis losses (average integral in the temperature range used for RC calculations) has been analyzed and compared with values reported in the literature. On table 3 the refrigeration capacity (RC), average hysteresis loss (HL_m) and effective

refrigeration capacity (RC_{eff}) obtained at magnetic fields of 2T, 4T and 6T are presented for comparison between disordered (AQ) and ordered (ORD) samples. This values confirm that the ordered alloy displays a higher RC and a lower hysteresis loss so, the RC_{eff} improves between 45 and 65% in ordered state with a negligible change in martensitic transformation temperature as shown before.

The RC_{eff} for ORD sample under 2T (a magnetic field that can be provided by a permanent magnet) is 86 J/kg, more than 15% higher than the largest values found in Ni–Mn-based alloys, such as $Ni_{45}Co_5Mn_{36}In_{13.3}Cu_{0.7}$ (63.8 J/kg) [15], $Ni_{40.6}Co_{8.5}Mn_{40.9}Sn_{10}$ (70 J/kg) [45] and $Ni_{48}Co_1Mn_{37}In_{14}$ (75 J/kg) [44]. At higher magnetic fields, i.e. at 6T the RC_{eff} reaches 314 J/kg, one of the highest reported values for magnetocaloric MMSMA operating at room temperature [15].

	RC [J/Kg]			HL_m [J/Kg]			RC_{eff} [J/Kg]		
	2T	4T	6T	2T	4T	6T	2T	4T	6T
AQ	81	200	316	22	76	122	59	124	192
ORD	103	253	397	17	61	83	86	192	314

Table 3: Calculated refrigeration capacity (RC), average hysteresis loss (HL_m) and effective refrigeration capacity (RC_{eff}) obtained at magnetic fields of 2T, 4T and 6T.

To compete with the efficiency of gas compressor-based systems and to improve the reversibility of the transformation, the reduction of magnetic losses (larger RC_{eff}) and thermal hysteresis are key factors [10, 11, 14, 15, 31, 46]. Figure 6 shows a summary of the main reported values of RC_{eff} and hysteresis found in literature for different magnetocaloric alloys operating between 260 and 330 k (range for room temperature cooling applications). Therefore, the further to the top-left in the figure of merit, the better the alloy will be for magnetic refrigeration. The ORD ordered sample (blue big circles) possesses an excellent combination of low thermal hysteresis and high RC_{eff} not achieved previously in metamagnetic shape memory alloys.

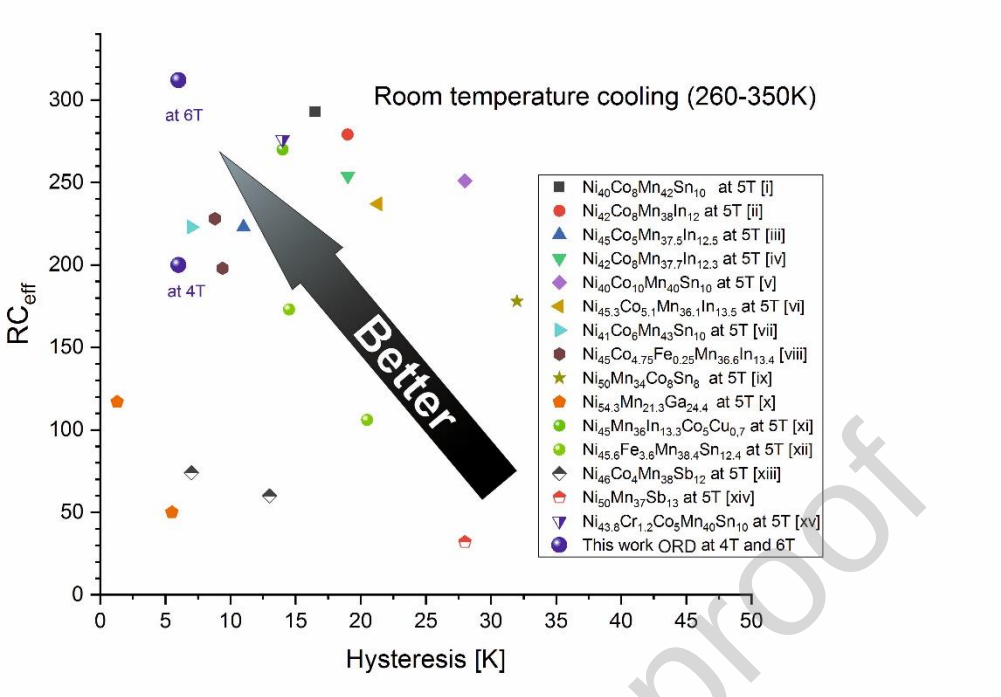

Figure 6: RC_{eff} and thermal hysteresis for different magnetocaloric alloys operating between 260 and 330 K, blue big circles correspond to the present ordered ORD Alloy at 4 and 6T. Data extracted from literature: i [43], ii [47], iii [42], iv [48], v [49], vi [50], vii [51], viii [52], ix [53], x [54], xi [15], xii [55], xiii [56], xiv [57], xv [58]

4. Conclusion

In this work, a Cu doped NiMnInCo alloy exhibiting a narrow thermal hysteresis (5-6K) at room temperature has been designed. The $L2_1$ atomic ordering produces an increase in the curie temperature of the austenite but hardly affects the martensitic transformation temperatures. On the ordered alloy, the magnetic hysteresis losses have been analyzed being one of the lowest reported in the literature for MMSMA. In parallel, the atomic order doubles the sensitivity of the transformation to magnetic fields, improves the magnetocaloric effect, the reversibility and enhances the refrigeration capacity. The effective cooling capacity coefficient RC_{eff} reaches 86 J/Kg for 2T and 314 J/Kg for 6T fields. Therefore, the ordered alloy possesses an excellent combination of low thermal hysteresis and high RC_{eff} not achieved previously in metamagnetic shape memory alloys. This work shows the remarkable importance of the study of the ordering effects in each new alloy designed and identifies a promising

way for the improvement of the properties of technological interest based on the magnetocaloric effect.

Acknowledgments

This work has been carried out with the financial support of the Spanish “Agencia Estatal de Investigación (AEI), Ministerio de Ciencia, Innovación y Universidades” (Projects number RTI2018-094683-B-C54 (MCIU/AEI/FEDER, UE)), Navarra Government (Project number PC017-018 AMELEC). P. La Roca has received funding from “la Caixa” and "Caja Navarra" Foundations, under agreement LCF/PR/PR13/51080004. We acknowledge ILL and SpINS for beam time allocation: experiment CRG-2856.

References

[1] International Energy Agency Report “The Future of Cooling: Opportunities for energy-efficient air conditioning” (2018)

[2] D. Coulomb, "Refrigeration and cold chain serving the global food industry and creating a better future: two key IIR challenges for improved health and environment," Trends in Food Science & Technology, vol. 19, 8, pp. 413-417, 2008.

[3] M. Balli, S. Jand, P. Fournier, A. Kedous-Lebouc, Advanced materials for magnetic cooling: Fundamentals and practical aspects, App. Phys. Rev. 4, 021305 (2017)

[4] N A Zarkevich, D D Johnson and V K Pecharsky, High-throughput search for caloric materials: the CaloriCool approach, J. Phys. D: Appl. Phys. 51 024002 (2018)

[5] O. Gutfleisch, M. A. Willard, E. Brück, C. H. Chen, S. G. Sankar, J. Ping Liu., Magnetic Materials and Devices for the 21st Century: Stronger, Lighter, and More

Energy Efficient. Advanced Materials, 23 821 (2011)

[6] J. Liu, T. Gottschall, K. P. Skokov, J. D. Moore, and O. Gutfleisch, Giant magnetocaloric effect driven by structural transitions, Nat. Mater. 11, 620 (2012).

[7] V. Franco, J.S. Blázquez, J.J. Ipus, J.Y. Law, L.M. Moreno-Ramírez, A. Conde., Magnetocaloric effect: From materials research to refrigeration devices Progress in Materials Science 93 112–232 (2018)

[8] X.Moya, E. Defay, V. Heine, N. D. Mathur, Too cool to work, Nature Physics 11, (2015) 202-205

[9] P. J. Shamberger and F. S. Ohuchi" Hysteresis of the martensitic phase transition in magnetocaloric-effect Ni-Mn-Sn alloys", PHYSICAL REVIEW B 79, 144407 (2009)

[10] J. Liu, Y. Gong, Y. You, X. You, B. Huang, X. Miao, G. Xu, F. Xu, E. Brück, Giant reversible magnetocaloric effect in MnNiGe-based materials: Minimizing thermal hysteresis via crystallographic compatibility modulation, Acta Materialia 174, (2019) 450-458

[11] T. Hess, L. M. Maier, N. Bachmann, P. Corhan, O. Schäfer-Welsen, J. Wöllenstein, K. Bartholomé, Thermal hysteresis and its impact on the efficiency of first-order caloric materials, J. Appl. Phys. 127, 075103 (2020)

[12] D. Zhao, J. Liu, X. Chen, W. Sun, Y. Li, M. Zhang, Y. Shao, H. Zhang, A. Yan, "Giant caloric effect of low-hysteresis metamagnetic shape memory alloys with exceptional cyclic functionality", Acta Materialia 133 (2017) 217-223

[13] D. Zhao, T. Castán, A. Planes, Z. Li, W. Sun, J. Liu, Enhanced caloric effect induced by magnetoelastic coupling in NiMnGaCu Heusler alloys: Experimental study and theoretical analysis, Physical Review B 96, 224105 (2017)

[14] Z. Li et al., "Tuning the Reversible Magnetocaloric Effect in Ni–Mn–In-Based Alloys through Co and Cu Co-Doping," Adv. Electron. Mater., vol. 5, no. 3, p. 1800845, 2019.

[15] H. Le Yan et al., “A strategy of optimizing magnetism and hysteresis simultaneously in Ni–Mn-based metamagnetic shape memory alloys,” Intermetallics, vol. 130, no. June 2020, p. 107063, 2021.

[16] X.-M. Huang, Y. Zhao, H.-L. Yan, N. Jia, B. Yang, Z. Li, Y. Zhang, C. Esling, X. Zhao, L. Zuo, Giant magnetoresistance, magnetostrain and magnetocaloric effects in a Cu-doped <001>-textured Ni45Co5Mn36In13.2Cu0.8 polycrystalline alloy, Journal of Alloys and Compounds 889 (2021) 161652

[17] X. Liang, J. Bai, J. Gu, J. Wang, H. Yan, Y. Zhang, C. Esling, X. Zhao, L. Zuo, Ab initio-based investigation of phase transition path and magnetism of Ni-Mn-In alloys with excess Ni or Mn, Acta Materialia 195 (2020) 109-122

[18] X. M. Sun, D. Y. Cong, Z. Li, Y. L. Zhang, Z. Chen, Y. Ren, K. D. Liss, Z. Y. Ma, R. G. Li, Y. H. Qu, Z. Yang, L.Wang, and Y. D. Wang, Manipulation of magnetostructural transition and realization of prominent multifunctional magnetoresponsive properties in NiCoMnIn alloys. Phys. Rev. Mater. 3, 034404 (2019).

[19] P. La Roca, P. Marinelli, A. Baruj, M. Sade, A. F. Guillermet, “Composition dependence of the Néel temperature and the entropy of the magnetic transition in the fcc phase of Fe-Mn and Fe-Mn-Co alloys”, Journal of Alloys and Compounds 688 594-598 (2016)

[20] J. Rodríguez-Carvajal, Recent advances in magnetic structure determination by neutron powder diffraction, Phys. B Condens. Matter. 192 (1993) 55–69, https:// doi.org/10.1016/0921-4526(93)90108-I

[21] V. Sánchez-Alarcos, V. Recarte, D.L.R. Khanna, J. López-García, J.I. Pérez-Landazábal, Deformation induced martensite stabilization in Ni45Mn36.7In13.3Co5 microparticles, Journal of Alloys and Compounds 870 (2021) 159536

[22] Sánchez-Alarcos V, Recarte V, Pérez-Landazábal JI, E. Cesari, Rodríguez-Velamazán JA, Long-Range Atomic Order and Entropy Change at the Martensitic

Transformation in a Ni-Mn-In-Co Metamagnetic Shape Memory Alloy, Entropy 16(5):2756-27675 (2014)

[23] V. Recarte, J.I. Perez-Landazabal, V. Sanchez-Alarcos , J.A. Rodrıguez-Velamazan“, Dependence of the martensitic transformation and magnetic transition on the atomic order in Ni–Mn–In metamagnetic shape memory alloys”, Acta Materialia 60 (2012) 1937–1945

[24] V. Sanchez-Alarcos, V. Recarte, J.I. Perez-Landazabal, C. Gomez-Polo, J.A. Rodrıguez-Velamazan, Role of magnetism on the martensitic transformation in Ni–Mn-based magnetic shape memory alloys, Acta Materialia 60 (2012) 459–468

[25] V. Recarte, J.I. Perez-Landazaba, V. Sanchez-Alarcos, V. Zablotski, E. Cesari, S. Kustov, Entropy change linked to the martensitic transformation in metamagnetic shape memory alloys, Acta Materialia 60 (2012) 3168-3175

[26] P. Czaja, J. Przewoznik, M. Kowalczyk, A. Wierzbicka-Miernik, J. Morgiel, and W. Maziarz, “Microstructural origins of martensite stabilization in Ni49Co1Mn37.5Sn6.5In6 metamagnetic shape memory alloy”, J. Mater. Sci. (2019) 54:4340–4353

[27] N.M. Bruno, D. Salas, S. Wang, I.V. Roshchin, R. Santamarta, R. Arroyave, T. Duong, Y.I. Chumlyakov, I. Karaman “On the microstructural origins of martensitic transformation arrest in a NiCoMnIn magnetic shape memory alloy”, Acta Mater, 142 (2018), pp. 95-106

[28] D. Salas, Y. Wang, T.C. Duong, V. Attari, Y. Ren, Y. Chumlyakov, R. Arróyave, I. Karaman, Competing Interactions between Mesoscale Length-Scales, Order-Disorder, and Martensitic Transformation in Ferromagnetic Shape Memory Alloys, Acta Materialia, 206,116616 (2021)

[29] U.S. Koshkidko, E.T. Dilmieva, A.P. Kamantsev, J. Cwik, K. Rogacki, A.V. Mashirov, V.V. Khovaylo, C. Salazar Mejia, M.A. Zagrebin, V.V. Sokolovskiy, V.D. Buchelnikov, P. Ari-Gur, P. Bhale, V.G. Shavrov, V.V. Koledov, Magnetocaloric effect and magnetic phase diagram of Ni-Mn-Ga Heusler alloy in steady and pulsed magnetic fields, Journal of Alloys and Compounds, 904, 164051 (2022)

[30] Z, Zhang, R,D. James, S. Muller, Energy barriers and hysteresis in martensitic phase transformations, Acta Materialia 57 (2009) 4332–4352.

[31] A. A. Mendonça, L. Ghivelder, P. L. Bernardo, Hanlin Gu, R. D. James, L. F. Cohen, and A. M. Gomes, “Experimentally correlating thermal hysteresis and phase compatibility in multifunctional Heusler alloys”, Phys. Rev. Materials 4, 114403 (2020)

[32] R.D. James and K.F. Hane. Martensitic transformations and shape-memory materials, Acta Materialia 48, 197 (2000)

[33] J. Cui J, Y. S. Chu, O. Famodu, Y. Furuya, J. Hattrick-Simpers, R. D. James, A. Ludwig, S. Thienhuas, M. Wutting, Z. Zhang, and I. Takechi, Combinatorial search of thermoelastic shape-memory alloys with extremely small hysteresis width, Nat. Mater. 5, 286 (2006).

[34] Y. Song, X. Chen, V. Dabade, T. W. Shield, and R. D. James, Enhanced reversibility and unusual microstructure of a phase-transforming material, Nature 502, 85 (2013).

[35] C. Chluba, W. Ge, R. L. de Miranda, J. Strobel, L. Kienle, E. Quandt, and M. Wuttig, Ultralow-fatigue shape memory alloy films, Science 348, 1004 (2015).

[36] K.K. Dubey, P. Devi, A. K. Singh, S. Singha “Improved crystallographic compatibility and magnetocaloric reversibility in Pt substituted Ni2Mn1.4In0.6 magnetic shape memory Heusler alloy”, Journal of Magnetism and Magnetic Materials 507 (2020) 166818

[37] Y. H. Qu, D. Y. Cong, X. M. Sun, Z. H. Nie, W. Y. Gui, R. G. Li, Y. Ren, and Y. D. Wang, Giant and reversible room-temperature magnetocaloric effect in Ti-doped Ni-Co-Mn-Sn magnetic shape memory alloys, Acta Materialia 134, 236 (2017).

[38] V. Khovailo, V. Novosad, T. Takagi, D. A. Filippov, R. Z. Levitin, A. N. Vasil’ev. , Magnetic properties and magnetostructural phase transitions in Ni2+xMn1-xGa shape memory alloys, Phys. Rev. B 70, 174413 (2004).

[39] L. Huang, D.Y. Cong, L. Ma, Z.H. Nie, Z.L. Wang, H.L. Suo, Y. Ren, Y.D. Wang, Large reversible magnetocaloric effect in a Ni-Co-Mn-in mangetic shape memory alloy, Appl. Phys. Lett. 108 (2016), 032405.

[40] Y.H. Qu, D.Y. Cong, S.H. Li, W.Y. Gui, Z.H. Nie, M.H. Zhang, Y. Ren, Y.D. Wang, Simultaneously achieved large reversible elastocaloric and magnetocaloric effects and their coupling in a magnetic shape memory alloy, Acta Materialia 151 (2018) 41-55

[41] T. Gottschall, K.P. Skokov, B. Frincu, and O. Gutfleisch,"Large reversible magnetocaloric effect in Ni-Mn-In-Co", APPLIED PHYSICS LETTERS 106, 021901 (2015).

[42] D. Bourgault, J. Tillier, P. Courtois, D. Maillard, X. Chaud, Large inverse magnetocaloric effect in Ni45Co5Mn37.5In12.5 single crystal above 300 K, Appl. Phys. Lett. 96 (2010) 132501.

[43] Z.B. Li, Z.Z. Li, J.J. Yang, B. Yang, X. Zhao, L. Zuo, Large room temperature adiabatic temperature variation in a Ni40Co8Mn42Sn10 polycrystalline alloy, Intermetallics 100 (2018) 57–62.

[44] L. Wang , Z. Li, J. Yang, B. Yang, X. Zhao, L. Zuo, "Large refrigeration capacity in a Ni48Co1Mn37In14 polycrystalline alloy with low thermal hysteresis", Intermetallics 125 (2020) 106888

[45] F. Chen, Y.X. Tong, L. Li, J.L.S. Llamazares, C.F. Sanchez-Valdes, P. Mullner, The effect of step-like martensitic transformation on the magnetic entropy change of Ni40.6Co8.5Mn40.9Sn10 unidirectional crystal grown with the Bridgman-Stockbarger technique, J. Alloys Compd. 691 (2017) 269–274.

[46] E. Stern-Taulats, P. O. Castillo-Villa, L. Mañosa, C. Frontera,S. Pramanick, S. Majumdar, A. Planes, Magnetocaloric effect in the low hysteresis Ni-Mn-In metamagnetic shape-memory Heusler alloy, Applied Physics Letters 106, 021901 (2015)

[47] F. Chen, Y.X. Tong, L. Li, J.L. Sanchez Llamazares, C.F. Sanchez-Valdes, P. Müllner, Broad first-order magnetic entropy change curve in directionally solidified polycrystalline Ni-Co-Mn-In, J. All. Compd. 727 (2017) 603–609.

[48] F. Cheng, L. Gao, Y. Wang, J. Wang, X. Liao, S. Yang, Large refrigeration capacity in a Ni42Co8Mn37.7In12.3 magnetocaloric alloy, J. Magn. Magn Mater. 478 (2019) 234–238.

[49] L. Huang, D.Y. Cong, H.L. Suo, Y.D. Wang, Giant magnetic refrigeration capacity near room temperature in Ni40Co10Mn40Sn10 multifunctional alloy, Appl. Phys. Lett. 104 (2014) 132407.

[50] Z.Z. Li, Z.B. Li, B. Yang, X. Zhao, Liang Zuo, Giant low-field magnetocaloric effect in a textured Ni45.3Co5.1Mn36.1In13.5 alloy, Scripta Mater. 151 (2018) 61–65.

[51] X.X. Zhang, H.H. Zhang, M.F. Qian, L. Geng, Enhanced magnetocaloric effect in Ni-Mn-Sn-Co alloys with two successive magnetostructural transformations, Sci. Rep. 8 (2018) 8235.

[52] L. Chen, F.X. Hu, J. Wang, L.F. Bao, J.R. Sun, B.G. Shen, J.H. Yin, L.Q. Pan, Magnetoresistance and magnetocaloric properties involving strong metamagnetic behavior in Fe-doped Ni45(Co1-xFex)5Mn36.6In13.4 alloys, Appl. Phys. Lett. 101 (2012), 012401.

[53] Z.B. Li, Y.W. Jiang, Z.Z. Li, C.F. Sanchez-Valdes, J.L. Sanchez Llamazares, B. Yang, Y.D. Zhang, C. Esling, X. Zhao, L. Zuo, Phase transition and magnetocaloric properties of Mn50Ni42-xCoxSn8 melt-spun ribbons, IUCrJ 5 (2018) 54–66.

[54] M. Qian, X. Zhang, Z. Jia, X. Wan, Lin Geng, Enhanced magnetic refrigeration capacity in Ni-Mn-Ga micro-particles, Materials and Design 148 (2018) 115–123

[55] H. Zhang, X. Zhang, M. Qian, L. Yin, L. Wei, D. Xing, J. Sun, L. Geng, Magnetocaloric effect in Ni–Fe–Mn–Sn microwires with nano-sized γ precipitates, Appl. Phys. Lett. 116 (6) (2020), 063904.

[56] R. Sahoo, D.M. Raj Kumar, D. Arvindha Babu, K.G. Suresh, A.K. Nigam, M. Manivel Raja, Effect of annealing on the magnetic, magnetocaloric and

magnetoresistance properties of Ni-Co-Mn-Sb melt spun ribbons, J. Magn. Magn Mater. 347 (2013), 95–100.

[57] M. Khan, N. Ali, S. Stadler, Inverse magnetocaloric effect in ferromagnetic Ni50Mn37+xSb13-x Heusler alloys, J. Appl. Phys. 101 (5) (2007), 053919.

[58] S. J. Kim, W. H. Ryu, H. S. Oh, E. S. Park, A large reversible room temperature magneto-caloric effect in Ni-TM-Co-Mn-Sn (TM = Ti, V, Cr) meta-magnetic Heusler alloys editors-pick, Journal of Applied Physics 123, 033903 (2018)

Credit author statement:

All authors participated on: Conceptualization, Methodology, Investigation, Data Curation and Writing the paper.

Declaration of interests

☒ The authors declare that they have no known competing financial interests or personal relationships that could have appeared to influence the work reported in this paper.

☐The authors declare the following financial interests/personal relationships which may be considered as potential competing interests:

Graphical abstract

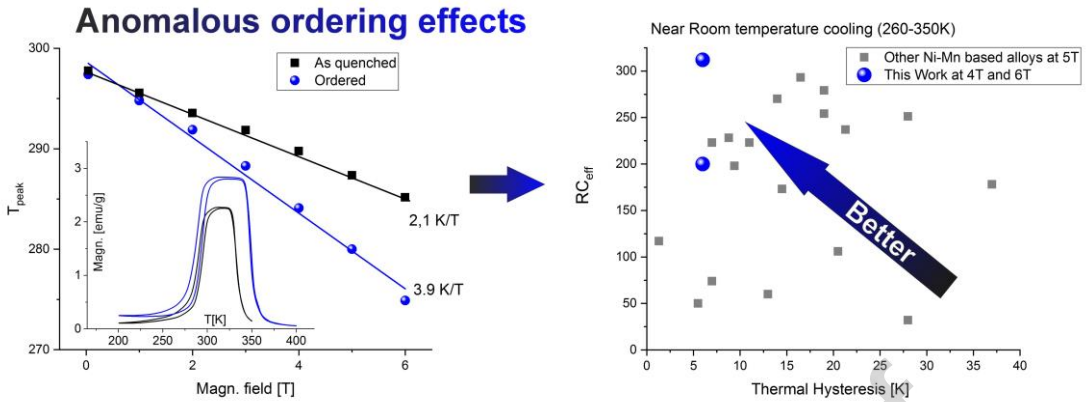

Highlights

1) Cu doped NiMnInCo MMSMA exhibiting a narrow thermal hysteresis (around 5 K) at room temperature has been obtained
2) An L_{21} ordering increases the magnetization of the austenite without changing the transformation temperatures.
3) The ordering doubles the sensitivity of the transformation to magnetic fields, improves the magnetocaloric effect, the reversibility and enhances the refrigeration capacity.
4) The ordered alloy displays an excellent combination of low thermal hysteresis and high Effective cooling capacity coefficient.